Modular Simulation Model for Falling Film Evaporators with Novel Approach to Manage Dominant Time-varying Transport Delays

Christian Schwaer[a,b], Julian Hofmann[b], Michael Mühlpfordt[c], Andreas Frank[c], Lutz Gröll[b]

[a] *Automation and Control Institute (ACIN), TU Wien, Gusshausstrasse 27-29, 1040 Vienna, Austria, email: schwaer@acin.tuwien.ac.at*

[b] *Institute of Applied Informatics, Karlsruhe Institute of Technology, Hermann-von-Helmholtz-Platz 1, 76344 Eggenstein-Leopoldshafen, Germany*

[c] *GEA Wiegand GmbH, Am Hardtwald 1, 76275 Ettlingen, Germany*

Abstract

Falling film evaporators with mechanical vapor recompression are widely used in food, chemical and pharmaceutical industries to concentrate liquids that contain solid content. This product diversity leads to a variety of different evaporator designs and operating points to achieve an indulgent as well as economic process.

In this paper, the evaporator is divided into design-independend subsystems to obtain a modular architecture. By introducing this modularity, numerous different evaporator designs, system parameters, operating points or control concepts can be configured and simulated. The plant operation or design can therefore be easily tested and costs for staff and experiments can be particularly reduced. A large challenge to create valid simulation tools consists of modeling the product transport within connecting pipes and during the evaporation process within the tubes, which in a dynamic process both lead to time-varying delays. As previously published models only include constant transport delays, they are disadvantageous to simulate real plant operation. In order to improve the simulation validity, a detailed dynamic full plant model is developed, which is able to illustrate dominant time-varying transport delays. A comparison with measured data of an existing falling film evaporator shows the validity of the proposed model.

Keywords: Falling Film Evaporator, Mechanical Vapor Recompression, Modular Simulation Model, Time-varying Transport Delay

1. Introduction

Falling film evaporators (FFEs) are industrial heat exchangers to concentrate solutions, suspensions or emulsions thermally by separating the volatile substance, often water, from the desired product. There are several different system designs of falling film evaporators with respect to the number of consecutive passes the product has to go through and the devices used to generate the necessary energy excess. However, a widely applied design is one with mechanical vapor recompression, i.e. the volatile substance is compressed mechanically and acts as the heating source for the evaporation process. Especially in the dairy industry, the concentrate will often be further processed in a spray dryer to produce powder. In this case, not all of the water in the product can be removed because of the loss of its properties as

Pre-print version of the article: C. Schwaer, J. Hofmann, M. Mühlpfordt, A. Frank and L. Gröll, "Modular simulation model for falling film evaporators with novel approach to manage dominant time-varying transport delays", *Computers and Chemical Engineering*, vol. 132, 2020. DOI: 10.1016/j.compchemeng.2019.106604

fluid due to the increasing product viscosity [1]. Therefore, the last stage in the powder production is always a drying process. However, the energy consumption of the spray dryer is 10-20 times higher per kg of removed water compared to the FFE [2]. Thus, it is reasonable to concentrate the product as much as possible in the FFE before drying.

Table 1: Symbols

Symbol	Description
A	Area (m^2)
c_p	Specific heat capacity ($J\ kg^{-1}K^{-1}$)
C_p	Heat capacity (JK^{-1})
d	Diameter (m)
D	Diffusion coefficient (m^2s^{-1})
Δh_v	Enthalpy of evaporation (Jkg^{-1})
η	Dynamic viscosity (Pas)
g	Gravitational constant (ms^{-2})
γ	Distribution coefficient (-)
h	Height (m)
k	Heat transfer coefficient ($Wm^{-2}K^{-1}$)
L	Length (m)
m	Mass (kg)
$\dot{m}$	Mass flow rate (kgs^{-1})
n	Number (-)
ν	Kinematic viscosity (m^2s^{-1})
N	Number of revolutions (s^{-1})
p	Pressure (bar)
P	Power (W)
$\dot{q}$	Heat flow rate (W)
Re	Reynolds number (-)
ϱ	Density (kgm^{-3})
s	Falling film thickness (m)
τ	Time delay (s)
ϑ	Temperature (°C)
v	Velocity (ms^{-1})
V	Volume (m^3)
$\dot{V}$	Volume flow (m^3s^{-1})
w_{dc}	Weight fraction dry content ($kgkg^{-1}$)
ζ	Discharge coefficient (-)

On the one hand, simulation models of FFEs are developed to get a deeper understanding of the process. On the other hand, costs, plant shutdowns and time can be efficiently reduced, as plant staff can be taught using a simulation model instead of the real plant. Moreover, novel developments concerning control concepts or system designs can be easily tested in a valid simulation environment, since there is less need for extensive experiments. In particular, modern control concepts based on the mathematical model, instead of widespread PID control

Pre-print version of the article: C. Schwaer, J. Hofmann, M. Mühlpfordt, A. Frank and L. Gröll, "Modular simulation model for falling film evaporators with novel approach to manage dominant time-varying transport delays", *Computers and Chemical Engineering*, vol. 132, 2020. DOI: 10.1016/j.compchemeng.2019.106604

Table 2: Subscripts

Subscript	Description
A	Ambience
C	Compressor
cond	Condensate
contr	Control
E	Effect
evap	Evaporation
fsh	Flash vapor
H	Heat chamber
init	Initial
inst	Instantaneous
j	Effect pass j
met	Metal
O	Orifice
p	Product
P	Distribution Plate
R	Reservoir
S	Separator
res	Resident
T	Tube
v	Vapor
virt	Virtual
w	Water

approaches, can be established. Among others, the latter facts indicate the significance of developing mathematical models to simulate the FFE process.

In the 1960's, first empirically-motivated [3] and ordinary differential equation (ODE) based [4] FFE simulation approaches were started. While other early computer programs to simulate multiple effect evaporators (MEEs) were considered unsuitable and gathered only few attention [5], first simple physically-motivated MEE models were implemented on digital computers [6, 7]. In this context, the nonlinear and linear simulation models of Newell and Fisher [8] could be experimentally evaluated. Another famous work in this early period was published by Andre and Ritter [9], who developed a dynamic FFE model of a two-effect evaporator based on material and energy balances, while neglecting fast dynamics. However, most of these early works only consider strongly simplified behavior of multiple effects and neglect other subsystems of FFEs. Moreover, they use lumped-parameter first-order ODEs to simulate both long- and short-tube evaporators. In 1990, Tonelli et al. [10] presented a computer package, where constant time-delays in and between the effects could be included into the simulation model.

More recent studies on dynamic FFE simulation focus on detailed subsystem modeling [11–13], usage of dynamic models for control design [14–16] or distributed-parameter effect models [17, 18]. However, constant transport velocity and thus constant delay is always assumed in these full plant simulation models. Other recent studies deal with modeling of

Pre-print version of the article: C. Schwaer, J. Hofmann, M. Mühlpfordt, A. Frank and L. Gröll, "Modular simulation model for falling film evaporators with novel approach to manage dominant time-varying transport delays", *Computers and Chemical Engineering*, vol. 132, 2020. DOI: 10.1016/j.compchemeng.2019.106604

special features, such as undesired fouling [19], pressure drop along the tubes and interactions between vapor and liquid phase [20] or turbulence in evaporating falling films [21]. In the latter paper, a fully partial differential equation (PDE) based model of evaporating falling film in a tube is implemented in FLUENT.

Besides dynamic simulation models, there are numerous publications on linear and non-linear steady-state MEE models with different main focuses, e.g. an estimation of the overall heat transfer coefficient [22], computational aspects [23, 24], multiple streams concepts [25, 26], usage of commercial software [27, 28], energy saving mechanisms in countercurrent MEEs [29], MEEs in the sugar industry [30] or energy reduction schemes [31]. Apart from physical modeling, pure empirically-motivated dynamic FFE models can be obtained using neural networks [32, 33] or identification-based black box approaches [1]. New experimental insights regarding the qualitative behavior of evaporating falling film are given in [34].

The main contribution of this paper is the enhancement of dynamic FFE subsystem models to enable simulation scenarios beyond static operating points. As, to the best of authors' knowledge, only constant delays within and between the effects are considered in the framework of full plant simulations [10–13, 18], a novel dynamic effect (time-variable delays within effects) and pipe model (time-variable delays between effects) to overcome this limitation is presented. Additionally, the derived subsystems are implemented as masked modules in Matlab/Simulink. Based on this modular architecture apporach, simulations of various FFE designs, e.g. different number of passes or different compressors, can be easily performed.

The rest of the paper is organized as follows. Section 2 introduces the system design of a FFE with four passes. The detailed subsystem model derivations are presented in Section 3. The simulation is executed and compared to measured data of the investigated FFE in Section 4. Section 5 finally concludes this paper.

2. System Design

Fig. 1 illustrates the general system design considered in this paper. The liquid is applied to the distribution plate which directs it to the effect where it flows downwards inside an arrangement of tubes as a continuous film. The tubes are heated from the outside, i.e. the liquid film starts to boil and evaporates partially, whereby it is concentrated and then reaches a reservoir at the bottom. In order to decrease the energy demand during evaporation and to achieve an optimal product concentration FFEs often have more than one pass. In this case, the obtained concentrate is taken out of the first reservoir and applied to a consecutive distribution plate, i.e. the product is passed through a series of consecutive plates, effects and reservoirs. However, the effects are connected in parallel from the view of the heat chamber since it embeds all present effects of the FFE.

In order to initialize the concentration process, steam referred to as $\dot{m}_{\mathrm{v,init}}$ is applied to the heat chamber and condenses on the tube's outside, leading to evaporation of the water within the product. The vapor evaporated within the effect is condensed by a compressor and directed into the heat chamber to ensure that the latent heat of vaporization basically origins from internally generated vapor. This guarantees the energy efficiency of the process.

Pre-print version of the article: C. Schwaer, J. Hofmann, M. Mühlpfordt, A. Frank and L. Gröll, "Modular simulation model for falling film evaporators with novel approach to manage dominant time-varying transport delays", *Computers and Chemical Engineering*, vol. 132, 2020. DOI: 10.1016/j.compchemeng.2019.106604

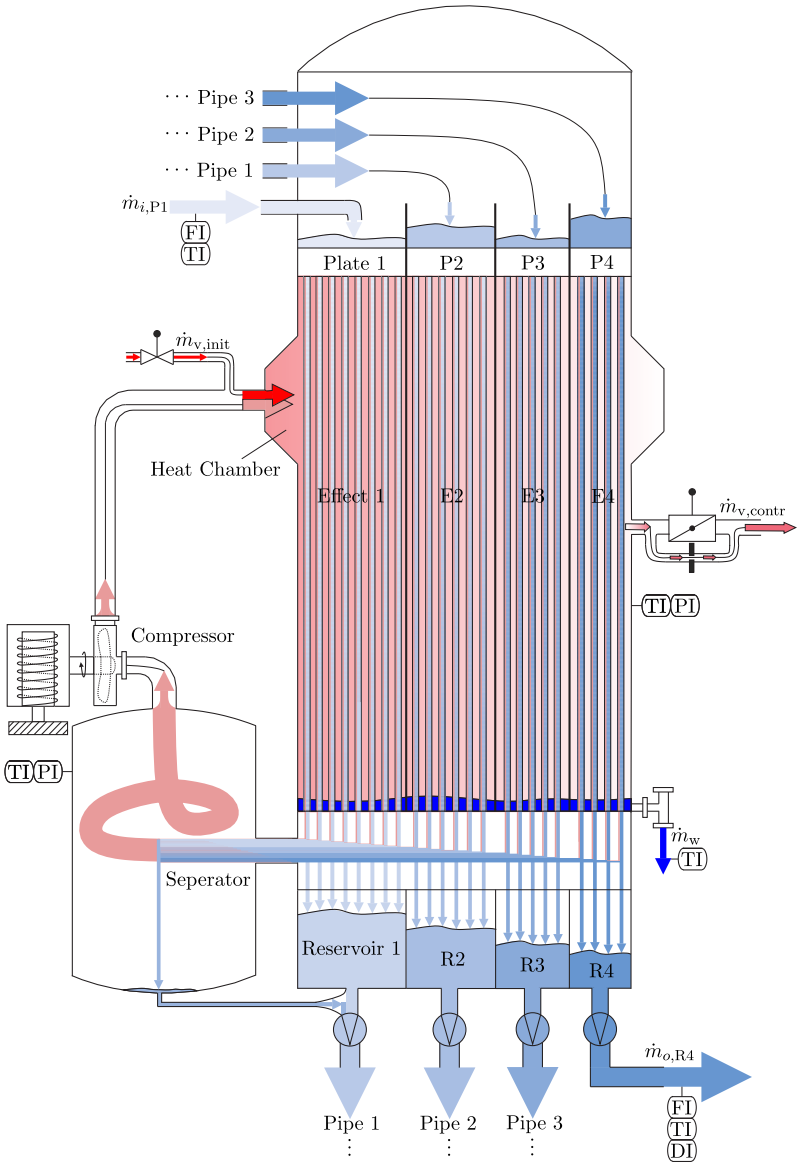

Figure 1: System design of the falling film evaporator with four passes and mechanical vapor recompression

3. Model Derivation

In this section all subsystems that form the whole evaporator are modeled. In general, the derived equations are formulated with case differentiations and exclusions of singular points to enable direct and easy implementation. Additionally, note that the index j, which used for indexing the passes, is mostly dropped for visibility purposes.

Pre-print version of the article: C. Schwaer, J. Hofmann, M. Mühlpfordt, A. Frank and L. Gröll, "Modular simulation model for falling film evaporators with novel approach to manage dominant time-varying transport delays", *Computers and Chemical Engineering*, vol. 132, 2020. DOI: 10.1016/j.compchemeng.2019.106604

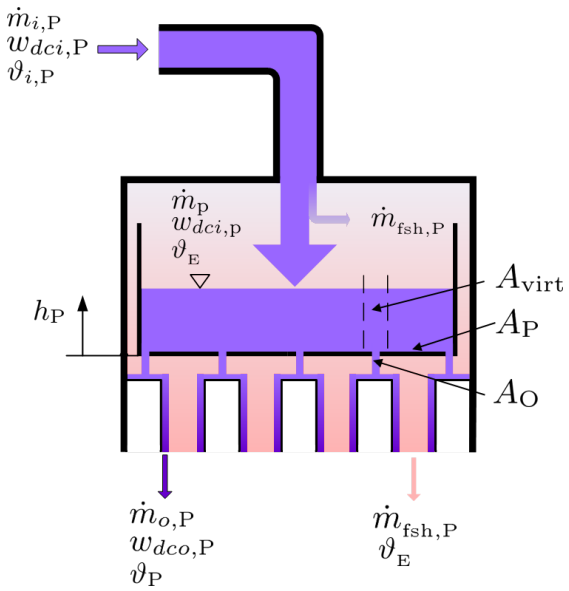

Figure 2: The distribution plate consists of a tank with holes in the bottom. An incoming product mass flow $\dot{m}_{i,\mathrm{P}}$ is applied and fills the tank, whereby the filling height is designated as h_{P}. Holes in the bottom distribute the product to the tubes of the following subsystem. The vapor mass flow $\dot{m}_{\mathrm{fsh}}$ occurs due to flashing of the overheated product. A_{virt} is the plate area A_{P} divided by the number of orifices.

3.1. Distribution Plate

The distribution plate consists of a tank to which the solution is applied, see Fig. 2. Through holes in the bottom of the tank the solution is distributed to the effect's tubes where it forms a thin falling film on the inside. Due to the low pressure inside the FFE and the fact that the solution is overheated when it enters the first distribution plate, the water within the product vaporizes instantaneously, forming the vapor mass flow $\dot{m}_{\mathrm{fsh}}$. Thus, the product cools down to effect temperature ϑ_{E} before entering the tank.

3.1.1. Total Mass Balance

The model derivation of the distribution plate follows [13]. However, the plate thickness is ignored since it has a much smaller influence on the filling height than the orifice edge shape, which has a large impact on the discharge coefficient [12]. Additionally, the derived equations are adapted to be applicable not only to a single stationary operating point. Using Bernoulli's law for the output mass flow, the equation of the filling height then becomes

$$\frac{\mathrm{d}}{\mathrm{d}t}h_{\mathrm{P}}(t) = \frac{\dot{m}_{\mathrm{p}}(t)}{\varrho_{\mathrm{P}}(t)A_{\mathrm{P}}} - \frac{\bar{A}}{A_{\mathrm{P}}}\sqrt{2g\,\max\{h_{\mathrm{P}}(t),0\}}, \tag{1}$$

resembling a first order low pass with

$$\bar{A} = \frac{n_{\mathrm{O}}\zeta_{\mathrm{O}}A_{\mathrm{O}}}{1-\left[\frac{A_{\mathrm{O}}}{A_{\mathrm{virt}}}\right]^2}. \tag{2}$$

Pre-print version of the article: C. Schwaer, J. Hofmann, M. Mühlpfordt, A. Frank and L. Gröll, "Modular simulation model for falling film evaporators with novel approach to manage dominant time-varying transport delays", *Computers and Chemical Engineering*, vol. 132, 2020. DOI: 10.1016/j.compchemeng.2019.106604

It is assumed that the temperature within the distribution plate is approximately the temperature within the effect ϑ_{E} and that the vapor as well as the product that reaches the plate adopt this temperature, see also Fig. 2. The mass flow of flashed vapor is determined by

$$\dot{m}_{\mathrm{fsh,P}}(t) = \begin{cases} \dfrac{\dot{m}_{i,\mathrm{P}}(t)c_p(t)\cdot[\vartheta_{i,\mathrm{P}}(t)-\vartheta_{\mathrm{E}}(t)]}{(c_{p,\mathrm{w}}-c_p(t))\vartheta_{\mathrm{E}}(t)+\Delta h_v(\vartheta_{\mathrm{E}}(t))} & \text{if } \vartheta_{i,\mathrm{P}} > \vartheta_{\mathrm{E}} \\ 0 & \text{else} \end{cases}, \tag{3}$$

such that the mass flow of product to the plate gets $\dot{m}_{\mathrm{p}}(t) = \dot{m}_{i,\mathrm{P}}(t) - \dot{m}_{\mathrm{fsh,P}}(t)$.

3.1.2. Dry Mass Balance

As mentioned, the start-up and shut-down processes of the FFE also have to be simulated, i.e. the differential equation of the product's weight fraction has to be adapted since it is a first order differential equation with a singular point at $h_{\mathrm{P}} = 0$. The equation then is

$$\frac{\mathrm{d}}{\mathrm{d}t}w_{dco,\mathrm{P}}(t) = \frac{\dot{m}_{\mathrm{p}}(t)}{\varrho_{\mathrm{P}}(t)A_{\mathrm{P}}\max\{h_{\mathrm{P}}(t),\epsilon\}}[w_{dci,\mathrm{p}}(t) - w_{dco,\mathrm{P}}(t)], \tag{4}$$

with a small constant $\epsilon > 0$ and $w_{dci,\mathrm{p}} = w_{dci,\mathrm{P}}\frac{\dot{m}_{i,\mathrm{P}}}{\dot{m}_{\mathrm{p}}}$. For instance, at the start-up process, when the product is applied to the distribution plate the filling level is zero and therefore the output's weight fraction of dry matter instantaneously adapts the weight fraction of the input because of $\frac{\mathrm{d}}{\mathrm{d}t}w_{dco,\mathrm{P}}(t) \to \infty$, i.e. the plate acts as a feedthrough with respect to the weight fraction. In this case is $h(t) < \epsilon$, so Eq. (4) becomes a very fast first order low pass that models the behavior in good approximation.

3.1.3. Energy Balance

Assuming negligible change of the product's specific heat capacity, the energy balance of the tank is

$$\frac{\mathrm{d}}{\mathrm{d}t}[C_{\mathrm{P}}(t)\vartheta_{\mathrm{P}}(t)] = \dot{m}_{\mathrm{p}}(t)c_{p,i}(t)\vartheta_{\mathrm{E}}(t) - \dot{m}_{o,\mathrm{P}}(t)c_p(t)\vartheta_{\mathrm{P}}(t), \tag{5}$$

where heat transfer to the ambience and between the distribution plates are neglected due to good insulation. The total heat capacity of the plate is given by

$$C_{\mathrm{P}}(t) = \varrho_{\mathrm{P}}(t)A_{\mathrm{P}}c_p(t)h_{\mathrm{P}}(t) + m_{\mathrm{met,P}}c_{p,\mathrm{met,P}}. \tag{6}$$

By applying the product rule and $\frac{\mathrm{d}}{\mathrm{d}t}c_p = \frac{\mathrm{d}}{\mathrm{d}t}\varrho_{\mathrm{P}} = 0$, the left side of Eq. (5) yields

$$\begin{aligned}\frac{\mathrm{d}}{\mathrm{d}t}[C_{\mathrm{P}}(t)\vartheta_{\mathrm{P}}(t)] = \varrho_{\mathrm{P}}(t)A_{\mathrm{P}}c_p(t)\vartheta_{\mathrm{P}}(t)\frac{\mathrm{d}}{\mathrm{d}t}h_{\mathrm{P}}(t) + (\varrho_{\mathrm{P}}(t)A_{\mathrm{P}}h_{\mathrm{P}}(t)c_p(t) \\ + m_{\mathrm{met,P}}c_{p,\mathrm{met,P}})\frac{\mathrm{d}}{\mathrm{d}t}\vartheta_{\mathrm{P}}(t).\end{aligned} \tag{7}$$

Combining Eq. (5) and (7) leads to

$$\frac{\mathrm{d}}{\mathrm{d}t}\vartheta_{\mathrm{P}}(t) = \frac{\dot{m}_{\mathrm{p}}(t)c_{p,i}(t)\vartheta_{\mathrm{E}}(t) - \vartheta_{\mathrm{P}}(t)[\dot{m}_{o,\mathrm{P}}(t)c_p(t) + \varrho_{\mathrm{P}}(t)A_{\mathrm{P}}c_p(t)\frac{\mathrm{d}}{\mathrm{d}t}h_{\mathrm{P}}(t)]}{\varrho_{\mathrm{P}}(t)A_{\mathrm{P}}c_p(t)h_{\mathrm{P}}(t) + m_{\mathrm{met,P}}c_{p,\mathrm{met,P}}}. \tag{8}$$

Pre-print version of the article: C. Schwaer, J. Hofmann, M. Mühlpfordt, A. Frank and L. Gröll, "Modular simulation model for falling film evaporators with novel approach to manage dominant time-varying transport delays", *Computers and Chemical Engineering*, vol. 132, 2020. DOI: 10.1016/j.compchemeng.2019.106604

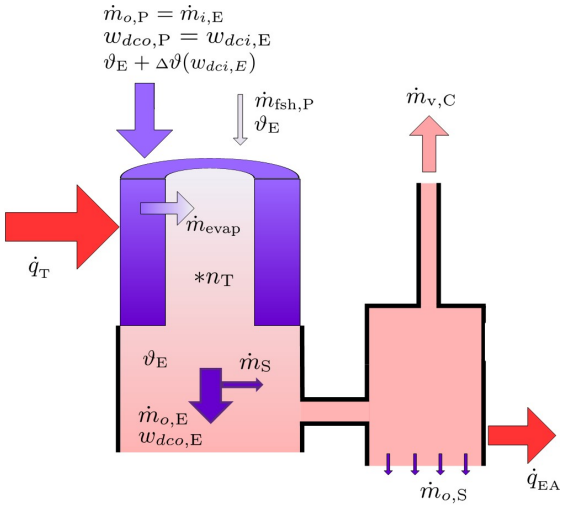

Figure 3: Schematic of the effect's mass and energy flows. At the top left the product and vapor mass flows entering the effect from the plate. During the product's residence within the tubes, the energy flow $\dot{q}_{\mathrm{T}}$ through the tubes causes an evaporation mass flow $\dot{m}_{\mathrm{evap}}$. At the bottom the concentrated product leaves the effect. A compressor absorbs the evaporated and flashed vapor $\dot{m}_{\mathrm{v,C}}$. Due to the high velocity of the vapor, a small part of product $\dot{m}_{\mathrm{S}}$ is carried away into the separator, which is neglected in the framework of this paper. Imperfect insulation results in an energy loss to ambience $\dot{q}_{\mathrm{EA}}$.

3.2. Effect

The product, which leaves the distribution plate, is fed to the effect where the solution flows downwards within tubes as a continuous film. Simultaneously, there is a heat flow through the wall of the tubes to evaporate the solvent, i.e. to concentrate the solution. As it flows down the tubes, an increasing amount of solvent is vaporized, such that the concentrated product leaves the tubes at the bottom. A schematic of this process is depicted in Fig. 3.

3.2.1. Total Mass Balance

The total mass balance, assuming a constant falling film velocity and constant evaporation along the tube, is given by the partial differential equation

$$\frac{1}{v_{\mathrm{T}}}\frac{\partial \dot{m}(x,t)}{\partial t} + \frac{\partial \dot{m}(x,t)}{\partial x} + \frac{1}{L_{\mathrm{T}}}\dot{m}_{\mathrm{evap}}(t) = 0, \tag{9}$$

that can be transformed into the differential equation with delays [11–13], i.e.

$$\dot{m}_{o,\mathrm{E}}(t) = \dot{m}_{i,\mathrm{E}}(t - \tau_{\mathrm{T}}) - \dot{\bar{m}}_{\mathrm{evap,res}}(t). \tag{10}$$

The last term is the mean of evaporation mass flow during residence of the product within the tubes

$$\dot{\bar{m}}_{\mathrm{evap,res}}(t) = \frac{1}{\tau_{\mathrm{T}}}\int_{t-\tau_{\mathrm{T}}}^{t} \dot{m}_{\mathrm{evap}}(t')\,\mathrm{d}t'. \tag{11}$$

Pre-print version of the article: C. Schwaer, J. Hofmann, M. Mühlpfordt, A. Frank and L. Gröll, "Modular simulation model for falling film evaporators with novel approach to manage dominant time-varying transport delays", *Computers and Chemical Engineering*, vol. 132, 2020. DOI: 10.1016/j.compchemeng.2019.106604

The instantaneous evaporation mass flow within effect pass j is determined by

$$\dot{m}_{\mathrm{evap},j} = \gamma_j \dot{m}_{\mathrm{v,C}} - \dot{m}_{\mathrm{fsh},j}, \tag{12}$$

where $\dot{m}_{\mathrm{v,C}}$ is the mass flow through the compressor, see Sec. 3.3.1, and γ_j a coefficient to back-calculate $\dot{m}_{\mathrm{v,C}}$ to each effect pass j. It is obtained by relating the heat flow into pass j to the total energy flow into all passes, i.e.

$$\gamma_j = \frac{\dot{q}_{\mathrm{T},j}}{\sum_{j=1}^{n} \dot{q}_{\mathrm{T},j}}. \tag{13}$$

3.2.2. Dry Mass Balance

The dry mass balance related to Eq. (10) is given by

$$w_{dco,\mathrm{E}}(t) = \frac{\dot{m}_{i,\mathrm{E}}(t-\tau_{\mathrm{T}}) w_{dci,\mathrm{E}}(t-\tau_{\mathrm{T}})}{\dot{m}_{i,\mathrm{E}}(t-\tau_{\mathrm{T}}) - \dot{m}_{\mathrm{evap,res}}(t)}. \tag{14}$$

3.2.3. Energy Balance

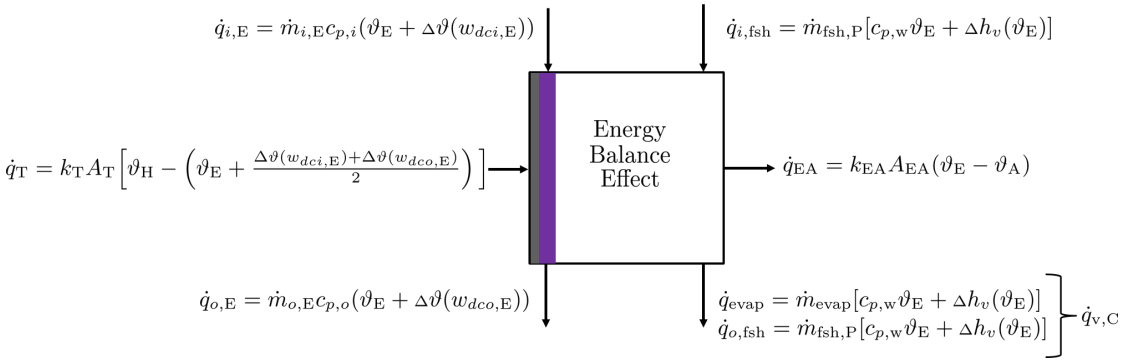

Figure 4: All energy flows entering and leaving the effect. The product (top left and bottom left), vapor (top right and bottom right), tube (left) as well as loss to ambience (right) are considered to determine the energy balance. In order to achieve a more accurate result, the boiling point elevation $\Delta\vartheta$ due to higher dry mass fraction of the product is added.

In literature on FFEs the considered product is mostly milk or dairy products [13, 14, 35]. In this case it is negligible that the presence of a solute with a specific weight fraction increases the boiling temperature of the solution [36]. However, in other products, e.g. glucose, the boiling point elevation has a larger impact, as it drastically influences the effect energy balance. Although the specific heat capacity slightly changes with time due to varying product temperature and dry mass fraction, it is assumed that $\frac{\mathrm{d}}{\mathrm{d}t} c_p = 0$. On the top and bottom left hand side in Fig. 4, the ingoing and outgoing product flows are displayed, which are both affected by the product's dry matter content and the resulting boiling point elevation. Since the energy flow through the tubes depend on the product temperature, it is approximated along the tubes by the mean of the ingoing and outgoing product temperatures. The energy

Pre-print version of the article: C. Schwaer, J. Hofmann, M. Mühlpfordt, A. Frank and L. Gröll, "Modular simulation model for falling film evaporators with novel approach to manage dominant time-varying transport delays", *Computers and Chemical Engineering*, vol. 132, 2020. DOI: 10.1016/j.compchemeng.2019.106604

resulting from vapor flows are shown on the top and bottom right hand side, respectively. The total outgoing vapor energy flow equals the energy flow through the compressor $\dot{q}_{\mathrm{v,C}}$. On the right hand side the energy loss due to heat conduction to ambience is depicted. As mentioned in Sec. 2, the effect passes are arranged in parallel which leads to the differential equation for the effect temperature

$$\frac{\mathrm{d}}{\mathrm{d}t}\vartheta_{\mathrm{E}} = \frac{\sum_{j=1}^{n}(\dot{q}_{i,\mathrm{E}} + \dot{q}_{\mathrm{T}})_{,j} - \sum_{j=1}^{n}(\dot{q}_{o,\mathrm{E}} + \dot{q}_{\mathrm{evap}})_{,j} - \dot{q}_{\mathrm{EA}} - \vartheta_{\mathrm{E}}\frac{\mathrm{d}m_{\mathrm{E}}}{\mathrm{d}t}c_p(\frac{w_{dci}+w_{dco}}{2})}{m_{\mathrm{E}}c_p\left(\frac{w_{dci}+w_{dco}}{2}\right) + m_{\mathrm{met,E}}c_{p,\mathrm{met}}}. \tag{15}$$

The time dependencies are dropped in this equation for better visibility and the expressions of the heat flows can be taken from Fig. 4. Furthermore, the total heat capacity of product in the effect is determined by the sum of product within the tubes of all passes

$$m_{\mathrm{E}}c_p\left(\frac{w_{dci}+w_{dco}}{2}\right) = \sum_{j=1}^{n} m_{\mathrm{T},j}c_p\left(\frac{w_{dci,E,j}+w_{dco,E,j}}{2}\right), \tag{16}$$

where $m_{\mathrm{T},j}$ follows from integrating $\frac{\mathrm{d}}{\mathrm{d}t}m_{\mathrm{T},j} = (\dot{m}_{i,\mathrm{E}} - \dot{m}_{\mathrm{evap}} - \dot{m}_{o,\mathrm{E}})_{,j}$.

3.2.4. Dynamic Effect Model

The previously made assumption of constant falling film velocity does not hold if the input mass flow is changed which is an important manipulable variable in driving and controlling the evaporator. Because of that, the Eqs. (10) and (14) with constant time delay do not represent the correct behavior of the FFE. For this reason a discrete model of a conveyor belt is developed as shown in Fig. 5. This model resembles a shift register that moves after every interval Δt, whereby Δt is the time discretization. Consequently, the mass reaches the tube's end after $\tau_{\mathrm{T}} = j\Delta t$, depending on the register j it was initially filled into. The amount of registers is determined by $n = \tau_{\mathrm{T,max}}/\Delta t$ with $\tau_{\mathrm{T,max}}$ as a reasonably chosen maximum time delay since $\tau_{\mathrm{T}} \to \infty$ if $\dot{m}_{i,\mathrm{E}} \to 0$, see Eq. (17). Using the amount of registers n and the tube's length L it follows that the spatial discretization is $\Delta x = L_{\mathrm{T}}/n$. The register j into which the mass is filled is calculated by dividing the instantaneous time delay by the time inverval $j = \tau_{\mathrm{T}}(t)/\Delta t$ with the time delay τ_{T} approximated by

$$\tau_{\mathrm{T}}(t) = \frac{V(t)}{\dot{V}(t)} = \frac{n_{\mathrm{T}}\pi L_{\mathrm{T}}(d_{i,\mathrm{T}} - s_{\mathrm{T}}(t))s_{\mathrm{T}}(t)\varrho_{i,\mathrm{E}}(t)}{\dot{m}_{i,\mathrm{E}}(t)}. \tag{17}$$

It depends on the thickness $s_{\mathrm{T}}(\dot{m}_{i,\mathrm{E}}, w_{dci,\mathrm{E}})$ of the falling film. Based on Nusselt's thin film theory, a formula, see [37], to determine s_{T} is given by

$$s_{\mathrm{T}} = \left(\frac{3\nu_{\mathrm{p}}^2}{g}\right)^{\frac{1}{3}} \mathrm{Re}_{\mathrm{p}}{}^{\frac{1}{3}} = \left(\frac{3\eta_{\mathrm{p}}^2}{g\varrho_{i,\mathrm{E}}^2}\right)^{\frac{1}{3}} \mathrm{Re}_{\mathrm{p}}{}^{\frac{1}{3}}, \tag{18}$$

$$\mathrm{Re}_{\mathrm{p}} = \frac{\dot{m}_{i,\mathrm{E}}}{n_{\mathrm{T}}\pi\eta_{\mathrm{p}}d_{i,\mathrm{T}}}. \tag{19}$$

The product has to be separated into water and dry matter since the models of the components differ with respect to the evaporation process. The water's discrete state-space

Pre-print version of the article: C. Schwaer, J. Hofmann, M. Mühlpfordt, A. Frank and L. Gröll, "Modular simulation model for falling film evaporators with novel approach to manage dominant time-varying transport delays", *Computers and Chemical Engineering*, vol. 132, 2020. DOI: 10.1016/j.compchemeng.2019.106604

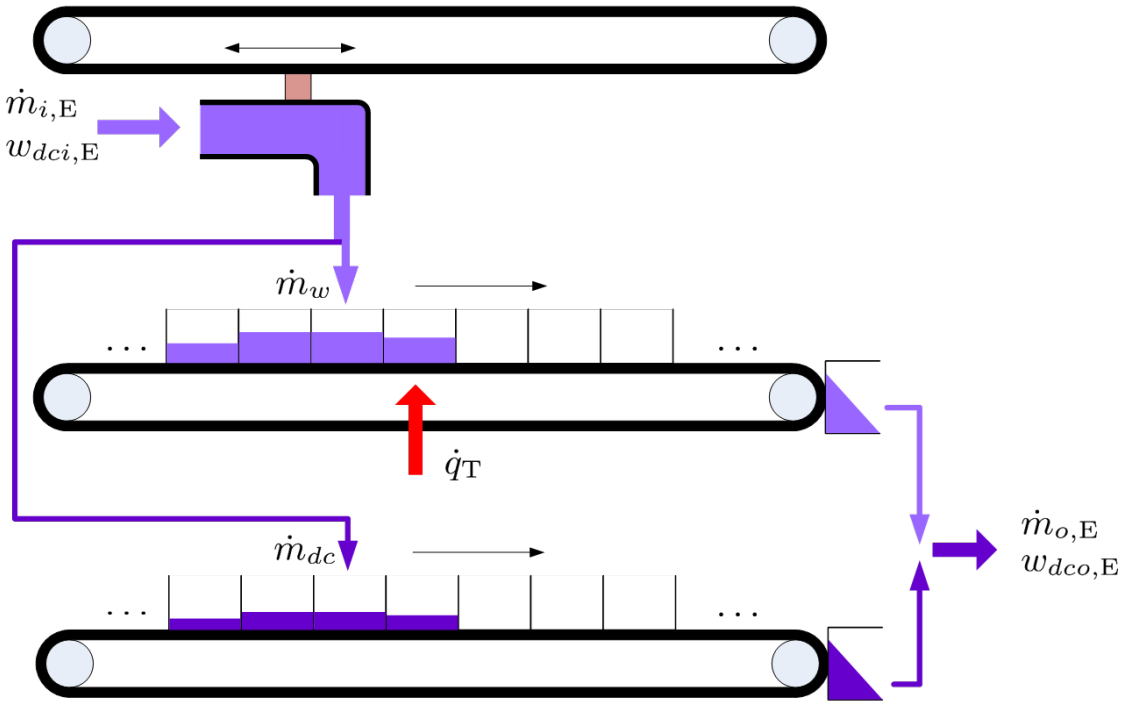

Figure 5: The dynamic effect model consists of two conveyor belts, one for water and one for dry matter. The number of containers on the belt can be chosen by the program user, as well as the time step after which the containers move one step further. Due to the evaporation process, the water mass within a specific container decreases to the end of the belt where water and dry matter are mixed again, thus creating a concentrated solution.

representation is

$$\begin{pmatrix} x_1 \\ x_2 \\ \vdots \\ x_n \end{pmatrix}_{i+1} = \begin{pmatrix} \xi & 1-2\xi & \xi & 0 & \cdots & 0 \\ 0 & \xi & 1-2\xi & \xi & \cdots & 0 \\ \vdots & \vdots & \vdots & \vdots & \ddots & \vdots \\ 0 & 0 & 0 & 0 & \cdots & \xi \end{pmatrix} \begin{pmatrix} x_1 \\ x_2 \\ \vdots \\ x_n \end{pmatrix}_i + \begin{pmatrix} b_1 \\ b_2 \\ \vdots \\ b_n \end{pmatrix}_i m_{\mathrm{w},i} - \begin{pmatrix} v_1 \\ v_2 \\ \vdots \\ v_n \end{pmatrix}_i m_{\mathrm{v},i}, \tag{20}$$

$$y_{\mathrm{w},i} = \begin{pmatrix} 1 & 0 & 0 & \dots & 0 \end{pmatrix} \underline{x}_i, \tag{21}$$

where the masses of water and vapor are determined by

$$m_{\mathrm{w},i} = \int_{t_i}^{t_i+\Delta t} (1 - w_{dci,\mathrm{E}}) \dot{m}_{i,\mathrm{E}}(\tau) \mathrm{d}\tau, \tag{22}$$

$$m_{\mathrm{v},i} = \int_{t_i}^{t_i+\Delta t} \dot{m}_{\mathrm{evap}}(\tau) \mathrm{d}\tau. \tag{23}$$

Pre-print version of the article: C. Schwaer, J. Hofmann, M. Mühlpfordt, A. Frank and L. Gröll, "Modular simulation model for falling film evaporators with novel approach to manage dominant time-varying transport delays", *Computers and Chemical Engineering*, vol. 132, 2020. DOI: 10.1016/j.compchemeng.2019.106604

The instantaneous evaporation mass flow $\dot{m}_{\text{evap}}$ is still determined by Eqs. (12) and (13). The dry matter model is the same as for water, see Eqs. (20)-(23), with the difference that the mass $m_{dc,i}$ is calculated by integrating the product $w_{dci,\text{E}}\dot{m}_{i,\text{E}}$ and $m_{\text{v},i} = 0$. In order to obtain the output mass flow $\dot{m}_{o,\text{E}}$, the masses of water and dry matter in the last register are summed and divided by Δt. The weight fraction of dry matter $w_{dco,\text{E},i}$ is the quotient of $m_{dc,i}$ and $m_{o,\text{E},i} = m_{dc,i} + m_{\text{w},i}$.

Consider Eq. (20) as the numerical treatment of the diffusion equation with $\xi = D\Delta t/\Delta x^2$. However, in the present case Δx and Δt to calculate ξ are not chosen independently since they are connected by $\Delta x = L_{\text{T}}/n = L_{\text{T}}\Delta t/\tau_{\text{T,max}}$. Hence,

$$\xi = \frac{D\Delta t}{\Delta x^2} = \frac{D\Delta t}{\left(\frac{L\Delta t}{\tau_{T,\max}}\right)^2} = \frac{D\tau_{T,\max}^2}{L^2\Delta t}. \tag{24}$$

As it is not a diffusion per se but rather a mass distribution within the tubes, the value of the diffusion coefficient D can not be found in literature. For this purpose, it can be used as an adaptive parameter to tune the model regarding the different products used. However, the Von Neumann stability analysis [38], which is used to check the stability of finite difference schemes and is based on the Fourier decomposition of numerical error demands

$$\xi = \frac{D\tau_{T,\max}^2}{L^2\Delta t} < \frac{1}{2}, \tag{25}$$

and consequently

$$D < \frac{L^2\Delta t}{2\tau_{T,\max}^2}. \tag{26}$$

3.3. Heat Chamber

The vaporised water is absorbed by a compressor which increases vapor temperature, thus creating a temperature difference between product and vapor. This gradient is used to induce a heat flow through the wall of the tubes to the solution as shown in Fig. 6. Within the chamber, the vapor condenses at the outside of the tubes, providing its condensation enthalpy to their walls.

3.3.1. Compressor

The compressor map describes the relationship between compressor speed, vapor suction flow and pressure difference of heat chamber and effect in one diagram as well as vapor suction flow and work done by the compressor in a second one. The algebraic equation for relating volume flow and compressor speed, similar to the derivation in [14], is

$$\frac{p_{\text{H}}(t) - p_{\text{E}}(t)}{\varrho_{\text{v,E}}(\vartheta_{\text{E}}(t))} = aN_{\text{C}}(t)^2 + bN_{\text{C}}(t)\dot{V}_{\text{v,C}}(t) + c\dot{V}_{\text{v,C}}(t)^2, \tag{27}$$

where $a - c$ are fitting coefficients to fit the equation to the compressor map. The pressures can be calculated by Antoine Equation [39] using the temperatures determined by related

Pre-print version of the article: C. Schwaer, J. Hofmann, M. Mühlpfordt, A. Frank and L. Gröll, "Modular simulation model for falling film evaporators with novel approach to manage dominant time-varying transport delays", *Computers and Chemical Engineering*, vol. 132, 2020. DOI: 10.1016/j.compchemeng.2019.106604

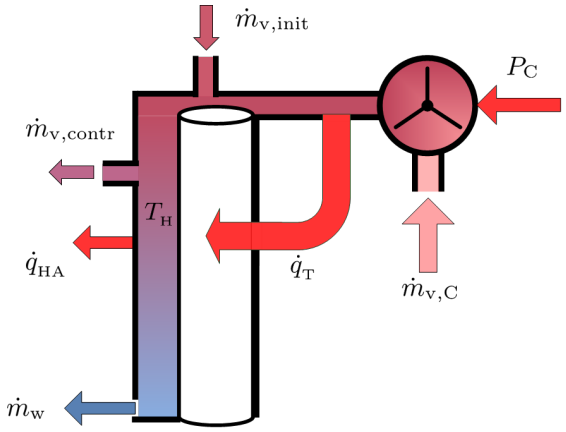

Figure 6: Mass and energy flows entering and leaving the heat chamber. The compressor sucks in the vapor $\dot{m}_{\mathrm{v,C}}$ and adds energy due to the supplied power. The vapor condenses on the tubes, providing the energy flow $\dot{q}_{\mathrm{T}}$ through the tube walls into the effect. The condensate is taken out of the chamber at the bottom. For temperature controlling purposes, the excess vapor mass flow $\dot{m}_{\mathrm{v,contr}}$ leaves the heat chamber through a valve. To start the evaporation process, the live steam mass flow $\dot{m}_{\mathrm{v,init}}$ is induced. Because of imperfect insulation there is also an energy loss $\dot{q}_{\mathrm{HA}}$ to the ambience.

energy balances. Since the compressor speed is known and the unknown variable is the volume flow, Eq. (27) can be expressed as

$$\dot{V}_{\mathrm{v,C}}(t) = \left(\frac{p_{\mathrm{H}}(t) - p_{\mathrm{E}}(t)}{\varrho_{\mathrm{v,E}}(\vartheta_{\mathrm{E}}(t))c} + \left(\frac{b^2 - 4ac}{4c^2} \right) N_{\mathrm{C}}(t)^2 \right)^{\frac{1}{2}} - \frac{b}{2c} N_{\mathrm{C}}(t). \tag{28}$$

The apparent ambiguity of the solution can be eliminated since the the energy flow that is inherent to the vapor mass flow has to be roughly equal to $\dot{q}_{\mathrm{T}}$, see Section 3.2.3. However, Eq. (28) only holds around the compressor's operating point. During the start-up process when the compressor speed is still small and the pressure p_{H} is increasing due to the application of external vapor $\dot{m}_{\mathrm{v,init}}$, the term under the square root can get negative. Because of that, a case differentiation is applied as follows

$$\dot{V}_{\mathrm{v,C}}(t) = \begin{cases} \left(\underbrace{\frac{p_{\mathrm{H}}(t) - p_{\mathrm{E}}(t)}{\varrho_{\mathrm{v,E}}(\vartheta_{\mathrm{E}}(t))c} + \left(\frac{b^2 - 4ac}{4c^2} \right) N_{\mathrm{C}}(t)^2}_{:=\text{radicand}} \right)^{\frac{1}{2}} - \frac{b}{2c} N_{\mathrm{C}}(t) & \text{radicand} > 0 \\ -\frac{b}{2c} N_{\mathrm{C}}(t) & \text{radicand} \leq 0 \end{cases}, \tag{29}$$

where $a, b > 0$ and $c < 0$. With the assumption that vapor behaves as an ideal gas, the vapor mass flow is then

$$\dot{m}_{\mathrm{v,C}}(t) = \dot{V}_{\mathrm{v,C}}(t) \varrho_{\mathrm{v,E}}(\vartheta_{\mathrm{E}}(t)). \tag{30}$$

The second algebraic equation describes the power supplied by the compressor and is adapted in the following way

$$P_{\mathrm{C}}(t) = d\varrho_{\mathrm{v,E}}(\vartheta_{\mathrm{E}}(t)) N_{\mathrm{C}}(t)^3 + e N_{\mathrm{C}}(t)^2 \dot{m}_{\mathrm{v,C}}(t) + f N_{\mathrm{C}}(t) \frac{\dot{m}_{\mathrm{v,C}}(t)^2}{\varrho_{\mathrm{v,E}}(\vartheta_{\mathrm{E}}(t))} + g \frac{\dot{m}_{\mathrm{v,C}}(t)^3}{\varrho_{\mathrm{v,E}}(\vartheta_{\mathrm{E}}(t))^2}, \tag{31}$$

Pre-print version of the article: C. Schwaer, J. Hofmann, M. Mühlpfordt, A. Frank and L. Gröll, "Modular simulation model for falling film evaporators with novel approach to manage dominant time-varying transport delays", *Computers and Chemical Engineering*, vol. 132, 2020. DOI: 10.1016/j.compchemeng.2019.106604

with the fitting coefficients $d - f$, since the equation given in [14] disregards the possibility of supplied power even if there is no mass flow which does not coincide with the compressor map.

3.3.2. Total Mass Balance

It is assumed that the incoming vapor distributes throughout the entire volume and condensates evenly along the tubes. Using these assumptions the total mass balance is given by

$$\frac{\mathrm{d}}{\mathrm{d}t}[\varrho A(s_{\mathrm{H}}(t))L_{\mathrm{T}}] = \dot{m}_{\mathrm{v,C}}(t) + \dot{m}_{\mathrm{v,init}}(t) - \dot{m}_{\mathrm{v,contr}}(t) - \dot{m}_{\mathrm{w}}(t). \tag{32}$$

The circular ring area depends on the film thickness s_{H}

$$A(s_{\mathrm{H}}) = n_{\mathrm{T}}\pi(d_{o,\mathrm{T}} + s_{\mathrm{H}}(t))s_{\mathrm{H}}(t)\ . \tag{33}$$

Substituting Eq. (33) into (32) and solving for the derivative of the film thickness yields

$$\frac{\mathrm{d}}{\mathrm{d}t}s_{\mathrm{H}}(t) = \frac{1}{n_{\mathrm{T}}\varrho\pi L_{\mathrm{T}}(d_{o,\mathrm{T}} + 2s_{\mathrm{H}}(t))}[\dot{m}_{\mathrm{v,C}}(t) + \dot{m}_{\mathrm{v,init}}(t) - \dot{m}_{\mathrm{v,contr}}(t) - \dot{m}_{\mathrm{w}}(s_{\mathrm{H}}(t))]. \tag{34}$$

For $\dot{m}_{\mathrm{v,init}}$ and $\dot{m}_{\mathrm{v,contr}}$ see Sec. 4.1 and Appendix A. The derivation of outgoing water mass flow follows [40] with the adaption to falling film on the tube's outer surfaces

$$\dot{m}_{\mathrm{w}}(s_{\mathrm{H}}(t)) = \frac{\pi\varrho g_z}{8\nu}\left(4(r_{o,\mathrm{T}} + s)^4 \ln\frac{r_{o,\mathrm{T}} + s}{r_{o,\mathrm{T}}} + 4r_{o,\mathrm{T}}^2(r_{o,\mathrm{T}} + s)^2 - r_{o,\mathrm{T}}^4 - 3(r_{o,\mathrm{T}} + s)^4\right). \tag{35}$$

Note that $r_{o,\mathrm{T}} = \frac{d_{o,\mathrm{T}}}{2}$, $\varrho = \varrho_{\mathrm{w,cond}}$, $\eta = \eta_{\mathrm{w,cond}}$ and $s = s_{\mathrm{H}}(t)$, what disagrees with the assumption of a steady flow in the derivation of Eq. (35). However, since $\frac{\mathrm{d}s}{\mathrm{d}t} \ll 1$, it can be considered that this assumption still holds.

3.3.3. Energy Balance

Assuming that the vapor's heat capacity is negligible in comparison to the capacity of water and metal as well as $\frac{\mathrm{d}}{\mathrm{d}t}c_{p,\mathrm{w}} = 0$, the energy balance of the heat chamber is evaluated. By solving the latter for the temperature, the first-order ODE

$$\frac{\mathrm{d}}{\mathrm{d}t}\vartheta_{\mathrm{H}}(t) = \frac{\dot{q}_{\mathrm{v,C}} + P_{\mathrm{C}} + \dot{q}_{\mathrm{v,init}} - \sum_{j=1}^{n}\dot{q}_{\mathrm{T},j} - \dot{q}_{\mathrm{w}} - \dot{q}_{\mathrm{HA}} - \dot{q}_{\mathrm{v,contr}} - \vartheta_{\mathrm{H}}\frac{\mathrm{d}m_{\mathrm{w}}}{\mathrm{d}t}c_{p,\mathrm{w}}}{m_{\mathrm{w}}c_{p,\mathrm{w}} + m_{\mathrm{met,H}}c_{p,\mathrm{met,H}}}, \tag{36}$$

is obtained, where

$$\dot{q}_{\mathrm{HA}}(t) = k_{\mathrm{HA}}A_{\mathrm{HA}}(\vartheta_{\mathrm{H}}(t) - \vartheta_{\mathrm{A}}(t)), \tag{37a}$$
$$\dot{q}_{\mathrm{w}}(t) = \dot{m}_{\mathrm{w}}(t)c_{p,\mathrm{w}}(t)\vartheta_{\mathrm{H}}(t), \tag{37b}$$
$$\dot{q}_{\mathrm{v,contr}}(t) = \dot{m}_{\mathrm{v,contr}}(t)\left(c_{p,\mathrm{w}}(t)\vartheta_{\mathrm{H}}(t) + \Delta h_v(\vartheta_{\mathrm{H}})\right), \tag{37c}$$
$$\dot{q}_{\mathrm{v,init}}(t) = \dot{m}_{\mathrm{v,init}}(t)\left(c_{p,\mathrm{w}}(t)\vartheta_{\mathrm{H}}(t) + \Delta h_v(\vartheta_{\mathrm{H}})\right). \tag{37d}$$

The compressor's power P_{C} is determined by Eq. (31).

Pre-print version of the article: C. Schwaer, J. Hofmann, M. Mühlpfordt, A. Frank and L. Gröll, "Modular simulation model for falling film evaporators with novel approach to manage dominant time-varying transport delays", *Computers and Chemical Engineering*, vol. 132, 2020. DOI: 10.1016/j.compchemeng.2019.106604

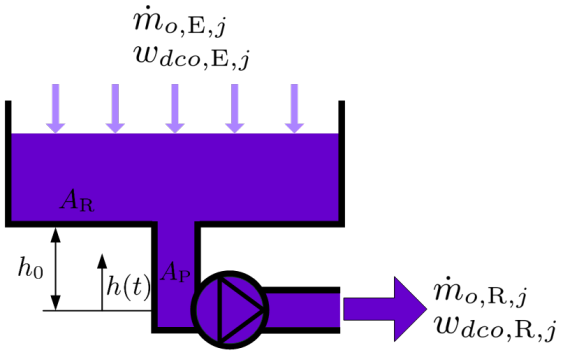

Figure 7: The product flows out of the effect into a reservoir which usually consist of a vertical pipe with area A_P and a tank with area A_R. A pump delivers the product into a pipe which directs it to the subsequent distribution plate.

3.4. Reservoir

The concentrated solution drops from the tubes to the bottom of the effect and a pump transports the product to the next pass, see Fig. 7. Two different cases can occur depending on the product used and the operating mode of the evaporator, i.e. how much product should be held as reserve: In the first case the filling level never reaches the reservoir and there is only product in the pipe. In the other case there is also product in the reservoir.

Furthermore, with respect to dry matter content two models are considered: the case of perfect mixing, which holds for solutions with small viscosity, and layering if viscosity increases due to higher concentration. Both cases can occur simultaneously within one plant, e.g. there is mixing in the first few passes and as the viscosity increases the layering model gives more accurate results in the later passes.

Since there is no significant temperature change along pipe and reservoir due to a good insulation, the product temperature is assumed constant in both of these subsystems.

3.4.1. Total Mass Balance

The total mass balance, considering the different areas of pipe and reservoir is given by

$$\frac{\mathrm{d}h(t)}{\mathrm{d}t} = \begin{cases} \dfrac{1}{\varrho_\mathrm{R}(t) A_\mathrm{Pipe}} (\dot{m}_{i,\mathrm{R}}(t) - \dot{m}_{o,\mathrm{R}}(t)) & \text{if } h(t) \leq h_0 \\ \dfrac{1}{\varrho_\mathrm{R}(t) A_\mathrm{R}} (\dot{m}_{i,\mathrm{R}}(t) - \dot{m}_{o,\mathrm{R}}(t)) & \text{if } h(t) > h_0 \end{cases}, \tag{38}$$

where the area of the reservoir can depend on the height, i.e. $A_\mathrm{R} = A_\mathrm{R}(h)$, if the reservoir has a conical instead of a cylindrical shape.

The output mass flow depends on the velocity of the pump. It is turned off if the filling height is smaller than the desired filling height and if the filling height is larger the mass flow is controlled by a PI controller, i.e.

$$\dot{m}_{o,\mathrm{R}}(t) = \max \left\{ k_\mathrm{P}(h(t) - h_d) + \int_0^t (h(\tau) - h_d) d\tau \ , \ 0 \right\}. \tag{39}$$

Pre-print version of the article: C. Schwaer, J. Hofmann, M. Mühlpfordt, A. Frank and L. Gröll, "Modular simulation model for falling film evaporators with novel approach to manage dominant time-varying transport delays", *Computers and Chemical Engineering*, vol. 132, 2020. DOI: 10.1016/j.compchemeng.2019.106604

3.4.2. Dry Mass Balance

In order to obtain the equation describing the dry mass balance in the case of mixing the same approach as in Sec. 3.1 is used. Again considering the two different cases it is given by

$$\text{Mixing}: \quad \frac{\mathrm{d}}{\mathrm{d}t} w_{dco,\mathrm{R}}(t) = \begin{cases} \dfrac{\dot{m}_{i,\mathrm{R}}(t)}{h(t)\varrho_{\mathrm{R}}(t)A_{\mathrm{Pipe}}}[w_{dco,\mathrm{E}}(t) - w_{dco,\mathrm{R}}(t)] & \text{if } 0 < h(t) \leq h_0 \\ \dfrac{\dot{m}_{i,\mathrm{R}}(t)}{(h(t)-h_0)\varrho_{\mathrm{R}}(t)A_{\mathrm{R}}}[w_{dco,\mathrm{E}}(t) - w_{dco,\mathrm{R}}(t)] & \text{if } h(t) > h_0 \end{cases}. \tag{40}$$

In case of layering the model of variable transport delay is applied, see Sec. 3.5.

The instantaneous delay based on the current volume flow can be written as

$$\text{Layering}: \quad \tau_{\mathrm{inst,R}}(t) = \frac{V(t)}{\dot{V}(t)} = \begin{cases} \dfrac{\varrho_{\mathrm{R}}(t)A_{\mathrm{Pipe}}h(t)}{\dot{m}_{o,\mathrm{R}}(t)} & \text{if } 0 < h(t) \leq h_0 \\ \dfrac{\varrho_{\mathrm{R}}(t)A_{\mathrm{R}}(h(t)-h_0)}{\dot{m}_{o,\mathrm{R}}(t)} & \text{if } h(t) > h_0 \end{cases}. \tag{41}$$

3.5. Pipe

Besides transport processes within effects, see Sec. 3.2, there are also transport processes between effects, i.e. from the reservoir of one pass to the distribution plate of the subsequent one. As FFEs with multiple effects are large-scale plants, the summed pipe length can amount to several kilometers. Hence, the transport between effects cannot be neglected. Obviously, transportation of a product always introduces a time delay. In order to model the transportation of a fluid with dry matter, the concept of variable transport delay is introduced. The corresponding Simulink implementation is presented in [41]. The time it takes for an incompressible fluid mass particle to travel from the input to the output of a pipe depends on the pipe's length and on the velocity of the particle. A formulation of this concept is shown in Fig. 8. The variable transport delay is expressed by the following delay differential equation (DDE):

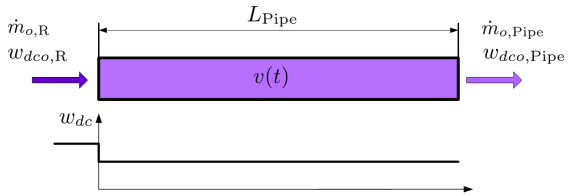

Figure 8: Formulation of the variable transport delay. A step in product concentration $w_{dco,\mathrm{R}}$ within the mass flow $\dot{m}_{o,\mathrm{R}}$ is applied at the beginning of the pipe. The time until the step reaches the end depends on the variable product velocity $v(t)$ during residence of the step within the tube.

$$\dot{\tau}_{\mathrm{Pipe}}(t) = 1 - \frac{\tau_{\mathrm{inst,Pipe}}(t - \tau_{\mathrm{Pipe}}(t))}{\tau_{\mathrm{inst,Pipe}}(t)}, \tag{42}$$

Pre-print version of the article: C. Schwaer, J. Hofmann, M. Mühlpfordt, A. Frank and L. Gröll, "Modular simulation model for falling film evaporators with novel approach to manage dominant time-varying transport delays", *Computers and Chemical Engineering*, vol. 132, 2020. DOI: 10.1016/j.compchemeng.2019.106604

with

$$\tau_{\text{inst,Pipe}}(t) = \frac{L_{\text{Pipe}}}{v(t)}, \tag{43}$$

$$v(t) = \frac{\dot{m}_{o,\text{R}}(t)}{\varrho(t) A_{\text{Pipe}}}, \tag{44}$$

and the initial funtion

$$\tau_{\text{Pipe}}(\phi) = \frac{L_{\text{Pipe}}}{v(0)} = \tau_{\text{inst,Pipe}}(0), \quad \phi \in [-\tau_{\text{inst,Pipe}}(0), 0]\,. \tag{45}$$

3.5.1. Total Mass Balance

In order to simulate start-up processes where $\dot{m}_{o,\text{Pipe}}(t) = \dot{m}_{o,\text{R}}(t)$ does not hold since the pipe is empty, the case differentiation

$$\dot{m}_{o,\text{Pipe}}(t) = \begin{cases} 0 & \text{if } \int_0^t \frac{\dot{m}_{o,\text{R}}(t')}{\varrho_{o,\text{R}}(t')} dt' < V_{\text{Pipe}} \\ \dot{m}_{o,\text{R}}(t) & \text{else} \end{cases}, \tag{46}$$

is implemented.

3.5.2. Dry Mass Balance

For the derivation of the outgoing dry mass concentration, the concept of variable transport delay is used, such that

$$w_{dco,\text{Pipe}} = w_{dco,\text{R}}(t - \tau_{\text{Pipe}}(t)). \tag{47}$$

4. Validation

In this section, the FFE model presented in Sec. 3 is validated by comparing simulated data with measured data from a real plant. As not all actuator signals are measured, the validation system is detailed in Sec. 4.1. Additionally, the plant simulation model is explained in Sec. 4.2 and corresponding results are discussed in Sec. 4.3.

4.1. Validation System

The considered validation system is depicted in Fig. 9. The plant inputs consist of the measured disturbances $z := \begin{bmatrix} w_{dci,\text{P1}} & \dot{m}_{i,\text{P1}} & \vartheta_{i,\text{P1}} \end{bmatrix}^\top$ and the effective (index e) actuator signals $u_{1,1} := \dot{m}_{\text{v,init},e}$, $u_{1,2} := \dot{m}_{\text{v,contr},e}$, $u_2 := N_{\text{C},e}$. The known signal $\tilde{u}_2 := N_{\text{C},d}$ describes the desired (index d) compressor speed, which is determined by a model predictive controller (MPC) controlling the product density $y_2 := \varrho_{o,\text{R4}}$ in the fourth reservoir. In this context, the PT_1 dynamic

$$T_\text{C} \frac{\text{d}u_2(t)}{\text{d}t} + u_2(t) = \tilde{u}_2(t), \quad u_2(0) = 0$$

represents the compressor actuator. Since $u_{1,1}$ and $u_{1,2}$ cannot be measured, the closed loop to control the effect temperature $y_1 := \vartheta_\text{E}$ must be included into the validation system. The desired effect temperature $y_{1,d}$ is a constant and depends on the considered product, hygienic

Pre-print version of the article: C. Schwaer, J. Hofmann, M. Mühlpfordt, A. Frank and L. Gröll, "Modular simulation model for falling film evaporators with novel approach to manage dominant time-varying transport delays", *Computers and Chemical Engineering*, vol. 132, 2020. DOI: 10.1016/j.compchemeng.2019.106604

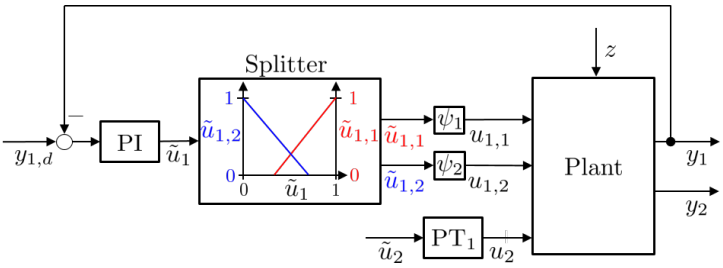

Figure 9: Validation system: On the one hand, it consists of the closed loop to control the effect temperature y_1 by applying PI control with split-range operation. The obtained valve positions $\tilde{u}_{1,1}$ and $\tilde{u}_{1,2}$ are converted into the live steam mass flow $u_{1,1}$ and the excess vapor mass flow $u_{1,2}$, respectively, via the dynamics ψ_1 and ψ_2. On the other hand, the validation system consists of further measured plant inputs, where z represents the input product dry mass fraction, mass flow and temperature. Additionally, the desired compressor speed $\tilde{u}_2$ is the known output of a MPC, where the PT_1 element describes the compressor's actuator dynamic generating the effective compressor speed u_2 to control the product density y_2 in the fourth reservoir.

and safety constraints as well as on the succeeding process. The control deviation enters a PI controller with $k_p = 1.8$, $k_i = 0.004\,\mathrm{s}^{-1}$ and anti reset windup, cf. [42], as well as a saturation with lower limit 0 und upper limit 1 to generate the signal $\tilde{u}_1 \in [0, 1]$. The latter is split into the live steam valve position $\tilde{u}_{1,1} \in [0, 1]$ and the excess vapor valve position $\tilde{u}_{1,2} \in [0, 1]$ using the following splitter characteristic

$$\tilde{u}_{1,2} = -\frac{20}{11}\tilde{u}_1 + 1, \quad \tilde{u}_1 \in [0, 0.55],$$
$$\tilde{u}_{1,1} = \frac{20}{11}\tilde{u}_1 - \frac{9}{11}, \quad \tilde{u}_1 \in [0.45, 1].$$

The valve positions enter the dynamics ψ_1 and ψ_2, which represent the valve characteristics and actuator dynamics of the live steam valve and the excess vapor valve, respectively. See Appendix A for further information. Thus, the corresponding effective mass flows are obtained. The plant simulation model itself is detailed in the following section.

4.2. Plant Simulation Model

In order to implement the simulation model, Matlab/Simulink is used. A major advantage of using Simulink is the possibility to transfer the modular design of the mathematical model into the simulation model. Corresponding parameters can be set via masks. Hence, masked modules for *Plate with Effect*, *Energy Balance Effect*, *Heat Chamber*, *Reservoir* and *Pipe* are developed. Fig. 10 illustrates the mask of a Heat Chamber module to give an example. Based on these elements, FFEs with arbitrary design, e.g. number of passes, can be simulated in a simple manner.

Firstly, note that the plate and effect model is combined under one mask, since all plate outputs only affect the subsequent effect and the number of plates corresponds to the number of effects. Additionally, the effect energy balance is implemented as extra module, since it gets inputs from each single effect. Secondly, the dynamic effect model, see Sec. 3.2.4, is used for validation purposes to get an online estimation of the time delay within effects.

In the application on hand, a FFE with four passes is considered. Thus, the simulation experiment's plant, which is referred to in Sec. 4.1, consists of four *Plate with Effect* (Eq. (1)

Pre-print version of the article: C. Schwaer, J. Hofmann, M. Mühlpfordt, A. Frank and L. Gröll, "Modular simulation model for falling film evaporators with novel approach to manage dominant time-varying transport delays", *Computers and Chemical Engineering*, vol. 132, 2020. DOI: 10.1016/j.compchemeng.2019.106604

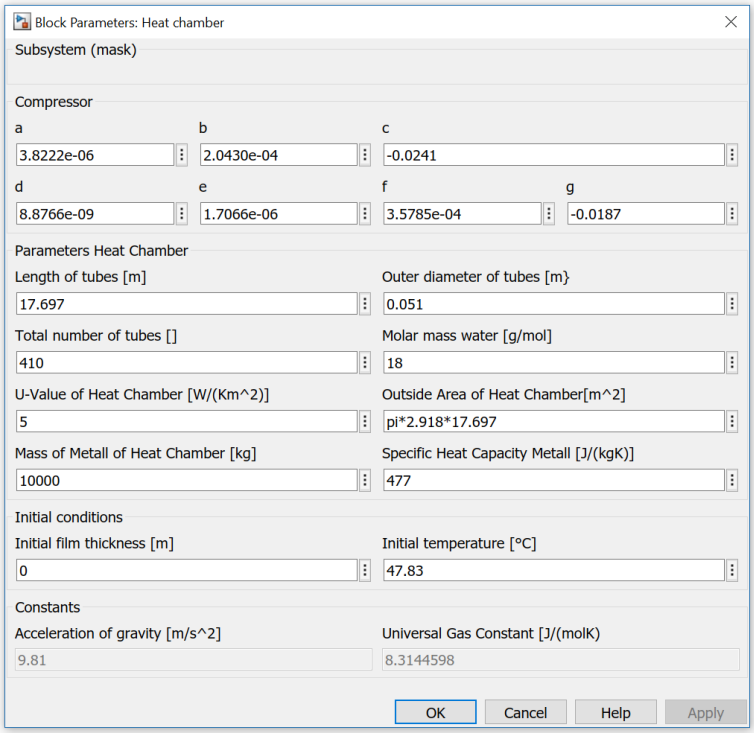

Figure 10: Simulink mask of a Heat Chamber module

to (8) and Eq. (17) to (26)) modules, which are each connected by *Pipe* (Eq. (42) to (47)) and *Reservoir* (Eq. (38) to (41)) modules, as well as one *Heat Chamber* (Eq. (27) to (37d)) and one *Energy Balance Effect* module (Eq. (15) to (16)). The plant simulation model is shown in Fig. 11.

4.3. Results and Discussion

In this section, the validation of the simulation model is performed by comparing simulated plant outputs against measured ones. As the disturbances z are known by measurements, the simulation model is fed by these measured inputs. While the control $\tilde{u}_2$ is known as it is the output of an MPC, the mass flows controlling the effect temperature are not recorded due to safety, effort and cost constraints. Hence, they are determined by including the effect temperature control loop, see Fig. 9, into the simulation model.
Due to the general model assumption that saturated vapor is the only gaseous medium in the FFE, the start-up process within the simulation is simplified as follows:

1. $t \in [0, 200]$ s: Water is induced onto plate 1 and flows through all passes for cleaning purposes (blue).

2. $t \in (200, 460]$ s: The live steam valve is fully opened, such that $\dot{m}_{\mathrm{v,init}}$ is induced at the pressure side of the compressor to heat up the effect tubes. Moreover, the compressor is started up (red).

Pre-print version of the article: C. Schwaer, J. Hofmann, M. Mühlpfordt, A. Frank and L. Gröll, "Modular simulation model for falling film evaporators with novel approach to manage dominant time-varying transport delays", *Computers and Chemical Engineering*, vol. 132, 2020. DOI: 10.1016/j.compchemeng.2019.106604

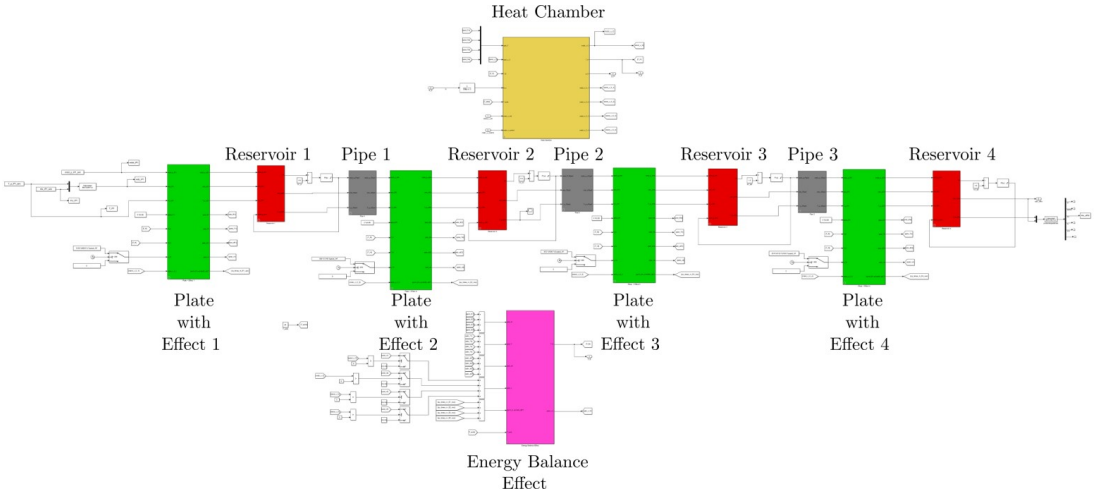

Figure 11: Plant Simulation Model

3. $t \in (460, 8260]\,\mathrm{s}$: The effect temperature control loop is active. Furthermore, product enters the evaporator instead of water at $t = 2000\,\mathrm{s}$, which can be concluded from Fig. 12b (green).

Note, that the colors inside the brackets of 1. to 3. refer to the background colors in Figures 12, 13 and 14, in order to illustrate the current process step. Also, in the real process there is only pure air as gaseous medium in the FFE at the beginning. After the air is vacuumed and the desired pressure is set, the product is induced and vapor expands until air and vapor phase are in thermodynamic equilibrium. However, since this process step cannot be simulated by the model, it has to be neglected in the framework of this paper.

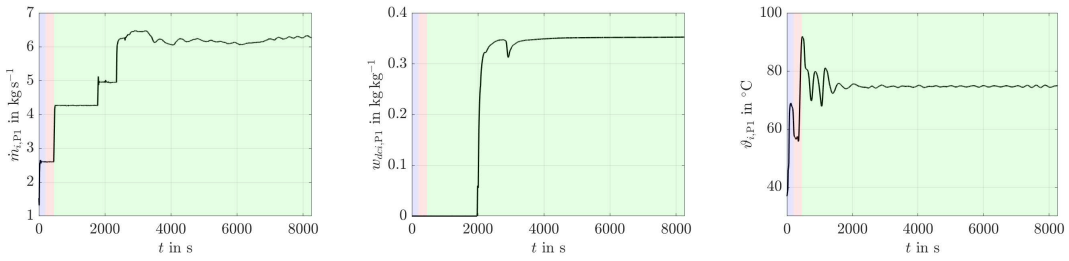

(a) Mass flow onto plate 1 (b) Dry mass fraction onto plate 1 (c) Temperature onto plate 1

Figure 12: Measured product input quantities (disturbances) for the simulated validation system

The simulated and measured effect temperature and heat chamber temperature are depicted in Fig. 14 and the final product density in Fig. 15. For the effect temperature shown in Fig. 14a, the dynamic and stationary behavior of simulated und measured signal are in good agreement. Nevertheless, the measured heat chamber temperature is approximately 1.5 °C lower than the simulated one, see Fig. 14b. This deviation can be explained by model and measurement uncertainty. Among others, the model uncertainty results from imperfect

Pre-print version of the article: C. Schwaer, J. Hofmann, M. Mühlpfordt, A. Frank and L. Gröll, "Modular simulation model for falling film evaporators with novel approach to manage dominant time-varying transport delays", *Computers and Chemical Engineering*, vol. 132, 2020. DOI: 10.1016/j.compchemeng.2019.106604

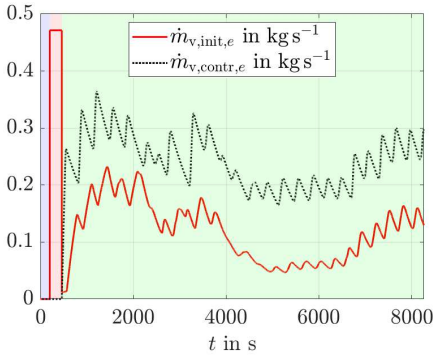

(a) Effective mass flows generated by closed effect temperature loop model

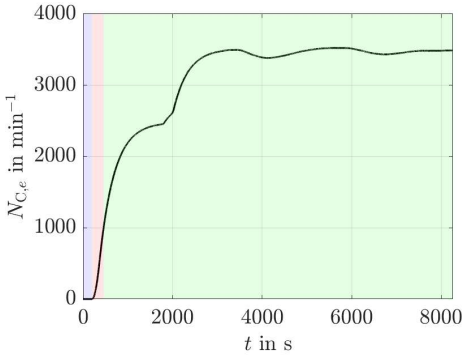

(b) Effective compressor speed generated by real MPC and PT_1 actuator dynamic

Figure 13: Controls of the simulated validation system

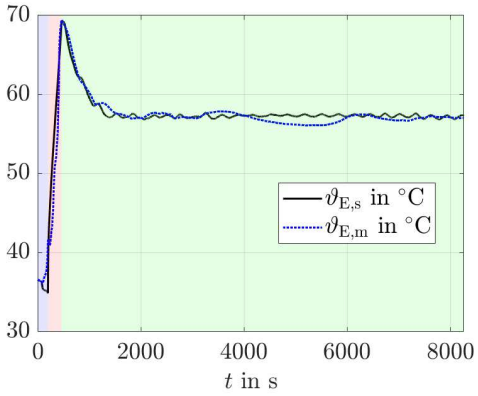

(a) Effect temperature

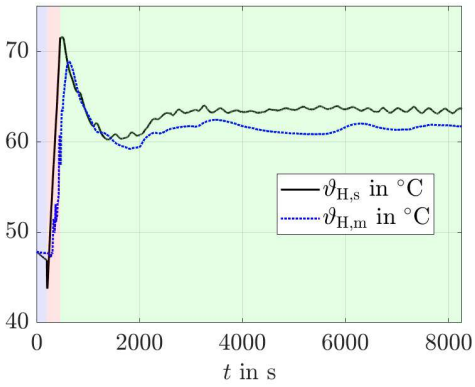

(b) Heat chamber temperature

Figure 14: Comparison of measured (index m) against simulated (index s) validation system outputs

estimations of constant heat transfer coefficients, which are actually time-varying due to varying amount of vapor on metal parts such as tubes, effect or heat chamber shells. On the one hand, the measurement uncertainty depends on the positioning of temperature sensors. On the other hand, there is an inherent measurement uncertainty of approximately 0.5 °C, since the considered medium is basically vapor, where the measurement of temperature is comparatively inexact. The observed oscillations in both simulated temperatures originate from the oscillations in the controlled mass flows as shown in Fig. 13a and cannot be detected in the measured ones due to the inertia of the corresponding measuring devices.

The final product density shown in Fig. 15 also maps the dynamic and stationary behavior of the real plant well. However, there is a remarkable deviation between measured and simulated data in the time delay along the whole plant of approximately 10%. In the model, time delays occur due to effect (see Sec. 3.2.4) and pipe (see Sec. 3.5) elements. Thus, the observed deviations can origin from neglected time delays in other plant elements, from model

Pre-print version of the article: C. Schwaer, J. Hofmann, M. Mühlpfordt, A. Frank and L. Gröll, "Modular simulation model for falling film evaporators with novel approach to manage dominant time-varying transport delays", *Computers and Chemical Engineering*, vol. 132, 2020. DOI: 10.1016/j.compchemeng.2019.106604

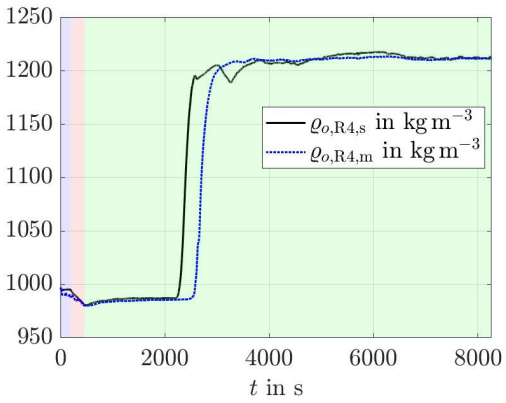

Figure 15: Product density in reservoir 4

uncertainties in effect and/or pipe delays, or from a mixture of both. Of course, by applying the static effect model, cf. Eq. (10) to Eq. (13), instead of the dynamic one, the constant time delays within the effects could have been adapted offline to perfectly fit the measured data. However, in an online environment, i.e. the simulation model is fed by the current real plant inputs, an offline adaption of constant effect delays would be impossible. Hence, it is emphasized that the developed model can be used as digital twin of a real FFE, since it is able to react dynamically to time-varying inputs.

5. Conclusion

In this study, a modular, physically-motivated simulation model for FFEs to handle time-varying transport delays is derived. A comparison with real plant data has shown that the dynamics and parameter values are accurately simulated.

Observed deviations with respect to the time delay along the whole plant offer and motivate future research. As in this study, the variable time delay along effect tubes only depends on product properties at the tube inputs although the product viscosity increases along the tubes, thus the velocity of the falling film decreases. Moreover, product incompressibility is assumed for the time-varying transport in pipe elements. In this context, it is questionable if this assumption still holds for increasing product concentrations. Thus, further studies on control-oriented transport modeling of fluids will follow to improve the time delay estimation along effect and pipe elements in order to not only create a digital twin of an existing FFE, but configure new FFE designs or features in advance.

Acknowledgments

This work has been supported in part by Institute for Automation and Applied Informatics, Karlsruhe Institute of Technology, as well as GEA Wiegand GmbH.

Pre-print version of the article: C. Schwaer, J. Hofmann, M. Mühlpfordt, A. Frank and L. Gröll, "Modular simulation model for falling film evaporators with novel approach to manage dominant time-varying transport delays", *Computers and Chemical Engineering*, vol. 132, 2020. DOI: 10.1016/j.compchemeng.2019.106604

References

[1] P. Quaak, M. van Wijck, J. van Haren, Comparison of process identification and physical modelling for falling-film evaporators, Food Control 5 (2) (1994) 73 – 82. doi:https://doi.org/10.1016/0956-7135(94)90089-2.
URL http://www.sciencedirect.com/science/article/pii/0956713594900892

[2] C. Ramirez, M. Patel, K. Blok, From fluid milk to milk powder: Energy use and energy efficiency in the european dairy industry, Energy 31 (12) (2006) 1984–2004.

[3] D. Johnson, Simulation and analysis improve evaporator control, ISA Journal 7 (7) (1960) 46.

[4] J. Andersen, L. Glasson, F. Lees, The control of a single-effect concentrating evaporator, Trans. Soc. Inst. Tech 13 (1) (1961) 21.

[5] A. Jernqvist, G. Olgard, B. Hedstrom, A digital computer program for multiple effect evaporation, SVENSK PAPPERSTIDNING-NORDISK CELLULOSA 69 (15) (1966) 477–+.

[6] P. Hussey, A digital computer model of a multiple effect evaporator, Proceedings of The South Afvican Sugar Technologists' Association-June 7 (1973) 1.

[7] U. Bolmstedt, Simulation of the steady-state and dynamic behaviour of multiple effect evaporation plants part 2: dynamic behaviour, Computer-Aided Design 9 (1) (1977) 29 – 40. doi:https://doi.org/10.1016/0010-4485(77)90060-4.
URL http://www.sciencedirect.com/science/article/pii/0010448577900604

[8] R. B. Newell, D. G. Fisher, Model development, reduction, and experimental evaluation for an evaporator, Industrial & Engineering Chemistry Process Design and Development 11 (2) (1972) 213–221.

[9] H. Andre, R. Ritter, Dynamic response of a double effect evaporator, The Canadian Journal of Chemical Engineering 46 (4) (1968) 259–264.

[10] S. M. Tonelli, J. Romagnoli, J. Porras, Computer package for transient analysis of industrial multiple-effect evaporators, Journal of Food Engineering 12 (4) (1990) 267 – 281. doi:https://doi.org/10.1016/0260-8774(90)90002-P.
URL http://www.sciencedirect.com/science/article/pii/026087749090002P

[11] P. Quaak, J. Gerritsen, Modelling dynamic behaviour of multiple-effect falling-film evaporators, Computer applications in chemical engineering.

[12] J. Winchester, Model based analysis of the operation and control of falling-film evaporators, Ph.D. thesis, Massey University, New Zealand (2000).

[13] S. Paramalingam, Modelling, optimisation and control of a falling-film evaporator, Ph.D. thesis, Massey University, New Zealand (2004).

Pre-print version of the article: C. Schwaer, J. Hofmann, M. Mühlpfordt, A. Frank and L. Gröll, "Modular simulation model for falling film evaporators with novel approach to manage dominant time-varying transport delays", *Computers and Chemical Engineering*, vol. 132, 2020. DOI: 10.1016/j.compchemeng.2019.106604

[14] J. Winchester, C. Marsh, Dynamics and control of falling film evaporators with mechanical vapour recompression, in: Proceedings of the American Control Conference, 1999, pp. 3600–3604.

[15] H. H. Bakker, C. Marsh, S. Paramalingam, H. Chen, Cascade controller design for concentration control in a falling-film evaporator, Food Control 17 (2006) 325–330.

[16] Z. Stefanov, K. A. Hoo, Control of a multiple-effect falling-film evaporator plant, Industrial & Engineering Chemistry Research 44 (9) (2005) 3146–3158. arXiv:https://doi.org/10.1021/ie049397w, doi:10.1021/ie049397w.
URL https://doi.org/10.1021/ie049397w

[17] Z. I. Stefanov, K. A. Hoo, Distributed parameter model of black liquor falling-film evaporators. 2. modeling of a multiple-effect evaporator plant, Industrial & Engineering Chemistry Research 43 (25) (2004) 8117–8132. arXiv:https://doi.org/10.1021/ie049611g, doi:10.1021/ie049611g.
URL https://doi.org/10.1021/ie049611g

[18] F. M. Bojnourd, M. A. Fanaei, H. Zohreie, Mathematical modelling and dynamic simulation of multi-effect falling-film evaporator for milk powder production, Mathematical and Computer Modelling of Dynamical Systems 21 (4) (2015) 336–358. arXiv:https://doi.org/10.1080/13873954.2014.980276, doi:10.1080/13873954.2014.980276.
URL https://doi.org/10.1080/13873954.2014.980276

[19] C. O. Daz-Ovalle, G. Gonzlez-Alatorre, J. F. Alvarado, Analysis of the dynamic response of falling-film evaporators considering fouling, Food and Bioproducts Processing 104 (2017) 124 – 136. doi:https://doi.org/10.1016/j.fbp.2017.05.007.
URL http://www.sciencedirect.com/science/article/pii/S0960308517300652

[20] M. Gourdon, E. Mura, Performance evaluation of falling film evaporators in the dairy industry, Food and Bioproducts Processing 101 (2017) 22–31.

[21] C. R. Kharangate, H. Lee, I. Mudawar, Computational modeling of turbulent evaporating falling films, International Journal of Heat and Mass Transfer 81 (2015) 52–62.

[22] S. ANGELETTI, M. MORESI, Modelling of multiple-effect falling-film evaporators, International Journal of Food Science & Technology 18 (5) (1983) 539–563.

[23] O. S. Zain, S. Kumar, Simulation of a multiple effect evaporator for concentrating caustic soda solution-computational aspects, Journal of chemical engineering of Japan 29 (5) (1996) 889–893.

[24] F. W. Koko, D. D. Joye, Design calculations for multiple-effect evaporators. 2. comparison of linear and nonlinear methods, Industrial & Engineering Chemistry Research 26 (1) (1987) 104–107. arXiv:https://doi.org/10.1021/ie00061a020, doi:10.1021/ie00061a020.
URL https://doi.org/10.1021/ie00061a020

Pre-print version of the article: C. Schwaer, J. Hofmann, M. Mühlpfordt, A. Frank and L. Gröll, "Modular simulation model for falling film evaporators with novel approach to manage dominant time-varying transport delays", *Computers and Chemical Engineering*, vol. 132, 2020. DOI: 10.1016/j.compchemeng.2019.106604

[25] A. Westerberg, J. Hillenbrand, The synthesis of multiple-effect evaporator systems using minimum utility insightsii. liquid flowpattern selection, Computers & Chemical Engineering 12 (7) (1988) 625 – 636, special Issue on Process Systems Engineering. doi:https://doi.org/10.1016/0098-1354(88)80004-8.
URL http://www.sciencedirect.com/science/article/pii/0098135488800048

[26] S. Khanam, B. Mohanty, Development of a new model for multiple effect evaporator system, Computers & Chemical Engineering 35 (10) (2011) 1983 – 1993. doi:https://doi.org/10.1016/j.compchemeng.2010.11.001.
URL http://www.sciencedirect.com/science/article/pii/S009813541000339X

[27] M. Munir, Y. Zhang, D. Wilson, W. Yu, B. Young, Modelling of a falling film evaporator for dairy processes, in: Chemeca 2014: Processing excellence; Powering our future. Barton, ACT:Engineers Australia, 2014, pp. 174–181.

[28] Y. Zhang, M. T. Munir, I. Udugama, W. Yu, B. R. Young, Modelling of a milk powder falling film evaporator for predicting process trends and comparison of energy consumption, Journal of Food Engineering 225 (2018) 26–33.

[29] Q. Ruan, H. Jiang, M. Nian, Z. Yan, Mathematical modeling and simulation of countercurrent multiple effect evaporation for fruit juice concentration, Journal of Food Engineering 146 (2015) 243 – 251. doi:https://doi.org/10.1016/j.jfoodeng.2014.09.015.
URL http://www.sciencedirect.com/science/article/pii/S026087741400377X

[30] D. Srivastava, B. Mohanty, R. Bhargava, Modeling and simulation of mee system used in the sugar industry, Chemical Engineering Communications 200 (8) (2013) 1089–1101. arXiv:https://doi.org/10.1080/00986445.2012.737876, doi:10.1080/00986445.2012.737876.
URL https://doi.org/10.1080/00986445.2012.737876

[31] S. Khanam, B. Mohanty, Energy reduction schemes for multiple effect evaporator systems, Applied Energy 87 (4) (2010) 1102 – 1111. doi:https://doi.org/10.1016/j.apenergy.2009.05.003.
URL http://www.sciencedirect.com/science/article/pii/S0306261909001780

[32] N. Russell, H. Bakker, R. Chaplin, A comparison of dynamic models for an evaporation process, Chemical Engineering Research and Design 78 (8) (2000) 1120 – 1128, separation Processes. doi:https://doi.org/10.1205/026387600528274.
URL http://www.sciencedirect.com/science/article/pii/S0263876200720053

[33] A. O. S. Costa, E. L. Lima, Modelling and control of an industrial multiple-effect evaporator system, Canadian Journal of Chemical Engineering 81.

[34] M. Gourdon, F. Innings, A. Jongsma, L. Vamling, Qualitative investigation of the flow behaviour during falling film evaporation of a dairy product, Experimental Thermal and Fluid Science 60 (2015) 9–19.

Pre-print version of the article: C. Schwaer, J. Hofmann, M. Mühlpfordt, A. Frank and L. Gröll, "Modular simulation model for falling film evaporators with novel approach to manage dominant time-varying transport delays", *Computers and Chemical Engineering*, vol. 132, 2020. DOI: 10.1016/j.compchemeng.2019.106604

[35] P. Cunningham, N. Canty, T. O'Mahony, B. O'Connor, D. O'Callaghan, System identification of a falling-film evaporator in the dairy industry, in: UK Automatic Control Conference, 2006, pp. 1–7.

[36] P. Atkins, J. de Paula, Physical Chemistry, W. H. Freeman, 2006.

[37] V. Gesellschaft, VDI-Waermeatlas, 10th Edition, Springer Berlin Heidelberg, Wiesbaden, 2005.

[38] C. Hirsch, Numerical Computation of Internal and External Flows Volume 1: Fundamentals of Numerical Discretization, John Wiley and Sons, Hoboken, New Jersey, 1988.

[39] J. G. Speight, Lange's Handbook of Chemistry, 17th Edition, McGraw-Hill Education Ltd., 2017.

[40] A. Padmanaban, Film thickness measurements in falling annular films, Master's thesis, University of Saskatchewan, Saskatoon (2006).

[41] F. Zhang, M. Yeddanapudi, Modeling and simulation of time-varying delays, mathworks.

[42] M. V. Kothare, P. J. Campo, M. Morari, C. N. Nett, A unified framework for the study of anti-windup designs, Automatica 30 (12) (1994) 1869–1883.

[43] H. Auinger, J. Ehmann, L. Grütesen, J. Heinrich, M. Huk, K. Jürgens, W. Klein, A. Kuhn, B. Kujawski, D. Metz, A. Muschet, A. Nagel, H. Peters, R. Rölli, C. Schindler, K. Scholl, M. Schwind, J. Seckler, V. Seppendorf, F. Valentin-Rumpel, M. Voß, VDI Richtlinien, VDI 2173: Strömungstechnische Kenngrößen von Stellgeräten und deren Bestimmung, Tech. Rep. VDI 2173, Verein Deutscher Ingenieure, ICS 23.060.40 (2018).

Appendix A. Valves

To simulate the closed effect temperature loop, two valves are modelled: a valve to induce the live steam mass flow $\dot{m}_{\mathrm{v,init}}$ (index 1, live steam valve) and a valve to release the excess vapor mass flow $\dot{m}_{\mathrm{v,contr}}$ (index 2, excess vapor valve). The model of these valves [43] essentially converts the splitter outputs $\tilde{u}_{1,1}$, $\tilde{u}_{1,2} \in [0,1]$ representing desiered valve positions into desired mass flows via

$$\begin{aligned}
\dot{m}_{\mathrm{v,init},d} &= \begin{cases} 31.62\, K_{V,1}(\tilde{u}_{1,1}) \left(\frac{v_{2,1}}{p_{1,1}-p_{1,2}}\right)^{-\frac{1}{2}}, & p_{1,2} > \frac{p_{1,1}}{2} \\ 31.62\, K_{V,1}(\tilde{u}_{1,1}) \left(\frac{2v_1^*}{p_{1,1}}\right)^{-\frac{1}{2}}, & p_{1,2} \leq \frac{p_{1,1}}{2} \end{cases}, \\
\dot{m}_{\mathrm{v,contr},d} &= \begin{cases} 31.62\, K_{V,2}(\tilde{u}_{1,2}) \left(\frac{v_{2,2}}{p_{2,1}-p_{2,2}}\right)^{-\frac{1}{2}}, & p_{2,2} > \frac{p_{2,1}}{2} \\ 31.62\, K_{V,2}(\tilde{u}_{1,2}) \left(\frac{2v_2^*}{p_{2,1}}\right)^{-\frac{1}{2}}, & p_{2,2} \leq \frac{p_{2,1}}{2} \end{cases}, \end{aligned} \tag{A.1}$$

where $K_{V,1}(\tilde{u}_{1,1})$ and $K_{V,2}(\tilde{u}_{1,2})$ are the corresponding valve characteristics. The specific volumes $v_{2,i} = v(p_{i,2}, \vartheta_{i,1})$ and $v_i^* = v(\frac{p_{i,1}}{2}, \vartheta_{i,1})$ with $i = 1, 2$ are determined by Matlab's

Pre-print version of the article: C. Schwaer, J. Hofmann, M. Mühlpfordt, A. Frank and L. Gröll, "Modular simulation model for falling film evaporators with novel approach to manage dominant time-varying transport delays", *Computers and Chemical Engineering*, vol. 132, 2020. DOI: 10.1016/j.compchemeng.2019.106604

`Xsteam.m`. In order to simulate the valve actuators, both $\dot{m}_{\mathrm{v,init},d}$ and $\dot{m}_{\mathrm{v,contr},d}$ each pass a PT_1 element to obtain the corresponding effective mass flows $u_{1,1}$ and $u_{1,2}$, i.e.

$$\begin{aligned} T_{\mathrm{V1}}\frac{\mathrm{d}u_{1,1}(t)}{\mathrm{d}t} + u_{1,1}(t) &= \dot{m}_{\mathrm{v,init},d}(t), \quad u_{1,1}(0) = 0, \\ T_{\mathrm{V2}}\frac{\mathrm{d}u_{1,2}(t)}{\mathrm{d}t} + u_{1,2}(t) &= \dot{m}_{\mathrm{v,contr},d}(t), \quad u_{1,2}(0) = 0. \end{aligned} \tag{A.2}$$

The dynamics ψ_1 and ψ_2 described in Sec. 4.1 combine Eq. (A.1) with Eq. (A.2).

Appendix B. Product Properties

The product to be concentrated has a large influence on the design of a FFE, e.g. the number of passes. Moreover, the effect and heat chamber temperatures have to be carefully adapted to the considered product. On the one hand, these temperatures should be high enough to evaporate the product, while on the other, too high temperatures might destroy the product. Additionally, the flow behavior strongly depends on changing product properties. Hence, they have to be included into the simulation model. To describe important product properties, the following equations are used

$$\begin{aligned} \varrho(\vartheta, w_{dc}) &= \underbrace{\left(\mathrm{A}_{\varrho,\mathrm{w}} + \mathrm{B}_{\varrho,\mathrm{w}}\frac{\vartheta}{\mathrm{K}} + \mathrm{C}_{\varrho,\mathrm{w}}\frac{\vartheta^2}{\mathrm{K}^2}\right)\frac{\mathrm{kg}}{\mathrm{m}^3}}_{=\varrho_{\mathrm{w}}(\vartheta)}\left(1 + \mathrm{A}_{\varrho}{w_{dc}}^{\mathrm{B}_{\varrho}}\right), \\ \Delta h_v(\vartheta) &= \mathrm{B}_h\left(\frac{1-\frac{\vartheta}{\mathrm{C}_h}}{1-\frac{\mathrm{A}_h}{\mathrm{C}_h}}\right)^{0.38}\frac{\mathrm{kJ}}{\mathrm{kg}}, \\ c_p(\vartheta, w_{dc}) &= \left(\mathrm{A}_c + \mathrm{B}_c\vartheta\right)w_{dc}\frac{\mathrm{kJ}}{\mathrm{kg}\cdot\mathrm{K}} + \underbrace{\left(\mathrm{A}_{c,\mathrm{w}} + \mathrm{B}_{c,\mathrm{w}}\vartheta + \mathrm{C}_{c,\mathrm{w}}\vartheta^2\right)\frac{\mathrm{kJ}}{\mathrm{kg}\cdot\mathrm{K}}}_{=c_{p,\mathrm{w}}(\vartheta)}\left(1 - w_{dc}\right), \\ \eta(\vartheta, w_{dc}) &= \exp\left(\mathrm{E}_\eta + \frac{\mathrm{F}_\eta}{\mathrm{C}_\eta w_{dc} + 1} + \mathrm{A}_\eta {w_{dc}}^{\mathrm{D}_\eta} - (\mathrm{B}_\eta w_{dc} + \mathrm{G}_\eta)(\vartheta - \vartheta_{\mathrm{amb}})\right)\mathrm{Pa}\cdot\mathrm{s}, \\ \Delta\vartheta(\vartheta, w_{dc}) &= \left(\mathrm{A}_\Delta {w_{dc}}^{\mathrm{B}_\Delta} + \mathrm{C}_\Delta w_{dc}\frac{\vartheta - 343.15}{100}\right)\mathrm{K}. \end{aligned}$$

Here, it is assumed that the considered product properties are mainly affected by the product temperature ϑ and the dry matter mass fraction w_{dc}. Additionally, note that the constants (A, B, C, etc.) are fitted by using data from experiments.

Pre-print version of the article: C. Schwaer, J. Hofmann, M. Mühlpfordt, A. Frank and L. Gröll, "Modular simulation model for falling film evaporators with novel approach to manage dominant time-varying transport delays", *Computers and Chemical Engineering*, vol. 132, 2020. DOI: 10.1016/j.compchemeng.2019.106604